

CRKSPH-COMPATIBLE DISCRETIZATION OF THE SUPG AND SAAF TRANSPORT EQUATIONS

Brody R. Bassett¹ and J. Michael Owen¹

¹Lawrence Livermore National Laboratory
7000 East Avenue, Livermore, CA, 94550

bassett4@llnl.gov, mikeowen@llnl.gov

1. INTRODUCTION

Smoothed particle hydrodynamics (SPH) is a meshless approach to hydrodynamics commonly used in astrophysics or for problems with unstable flows [1]. There are several published methods for doing radiation hydrodynamics using SPH with radiation diffusion [2,3,4,5,6], including an implementation in the code used in this paper [7]. The radiation transport equation has also been solved using collocation methods [8,9,10,11,12,13] and variational forms [14,15].

Here we discretize the self-adjoint angular flux (SAAF) [16] and streamline-upwind Petrov-Galerkin (SUPG) [17] transport equations using reproducing kernels (RK) [18] with the collocation method to produce a discretization that is compatible with conservative reproducing kernel smoothed particle hydrodynamics (CRKSPH) [19] to permit future research into meshless radiation hydrodynamics. The novelty of this approach is a strong form discretization of the radiation transport equation that does not involve explicit integration and includes kernels that can reproduce functions up to an arbitrary polynomial order using reproducing kernels.

2. MESHLESS KERNELS

2.1. SPH Kernels

A standard SPH kernel W and its spatial derivatives can be written in terms of a base kernel in reference space W^b as

$$W(x, H) = W^b(\chi(\eta(x, H))), \quad (1)$$

$$\partial_x^\alpha W = \xi^\alpha \partial_\chi W^b, \quad (2)$$

$$\partial_x^{\alpha\beta} W = \frac{H^{\alpha\gamma} H^{\beta\gamma} - \xi^\alpha \xi^\beta}{\chi} \partial_\chi W + \xi^\alpha \xi^\beta \partial_{\chi, \chi} W, \quad (3)$$

with the transformed distance vector in ASPH space η , the scaled distance χ , and the normalized distance vector ξ ,

$$\eta^\alpha = H^{\alpha\beta} x^\beta, \quad (4)$$

$$\chi = \sqrt{\eta^\alpha \eta^\alpha}, \quad (5)$$

$$\xi^\alpha = \frac{\eta^\beta}{\chi} H^{\alpha\beta}. \quad (6)$$

The SPH kernel centered at the point x_j and evaluated at the point x_i is written as

$$W_{ij} = W_j(x_i) = W(x_i - x_j, H_j). \quad (7)$$

SPH functions can be used to interpolate,

$$f_{\text{SPH}}(x) \approx \sum_j V_j f(x_j) W_j(x), \quad (8)$$

where V_j is the weight or volume of the kernel, but have a few issues when used to discretize partial differential equations. The interpolant cannot in general even reproduce a constant exactly, $\sum_j V_j W_j(x) \neq \text{const}$, which reduces accuracy and leads to issues near boundaries.

2.2. RK Kernels

To remedy these issues, the SPH functions can be augmented by RK, which can interpolate up to the chosen order of polynomial exactly. Defining $P(x)$ as the vector of polynomials with degree less than or equal to the chosen order [or $P_{ij} = P(x_i - x_j)$ once evaluated] and C_i as the corrections vector for the evaluation point i , the RK functions and their first two derivatives are defined as

$$U_{ij} = P_{ij}^\top C_i W_{ij}, \quad (9)$$

$$\partial_{x_i}^\alpha U_{ij} = \left(\partial_{x_i}^\alpha P_{ij}^\top C_i + P_{ij} \partial_{x_i}^\alpha C_i \right) W_{ij} + P_{ij}^\top C_i \partial_{x_i}^\alpha W_{ij}, \quad (10)$$

$$\begin{aligned} \partial_{x_i}^{\alpha\beta} U_{ij} = & \left(\partial_{x_i}^{\alpha\beta} P_{ij}^\top C_i + \partial_{x_i}^\beta P_{ij}^\top \partial_{x_i}^\alpha C_i + \partial_{x_i}^\alpha P_{ij}^\top \partial_{x_i}^\beta C_i + P_{ij}^\top \partial_{x_i}^{\alpha\beta} C_i \right) W_{ij} + P_{ij}^\top C_i \partial_{x_i}^{\alpha\beta} W_{ij} \\ & + \left(\partial_{x_i}^\alpha P_{ij}^\top C_i + P_{ij}^\top \partial_{x_i}^\alpha C_i \right) \partial_{x_i}^\beta W_{ij} + \left(\partial_{x_i}^\beta P_{ij}^\top C_i + P_{ij}^\top \partial_{x_i}^\beta C_i \right) \partial_{x_i}^\alpha W_{ij}, \end{aligned} \quad (11)$$

where $U_{ij} = U_j(x_i)$ is the kernel U_j evaluated at the point x_i . The corrections vectors are defined as

$$C_i = M_i^{-1} G, \quad (12)$$

$$\partial_{x_i}^\alpha C_i = -M_i^{-1} \partial_{x_i}^\alpha M_i C_i, \quad (13)$$

$$\partial_{x_i}^{\alpha\beta} C_i = -M_i^{-1} \left(\partial_{x_i}^{\alpha\beta} M_i C_i + \partial_{x_i}^\alpha M_i \partial_{x_i}^\beta C_i + \partial_{x_i}^\beta M_i \partial_{x_i}^\alpha C_i \right), \quad (14)$$

where

$$M_i = \sum_j V_j P_{ij} P_{ij}^\top W_{ij}, \quad (15)$$

$$\partial_{x_i}^\alpha M_i = \sum_j V_j \left[\left(\partial_{x_i}^\alpha P_{ij} P_{ij}^\top + P_{ij} \partial_{x_i}^\alpha P_{ij}^\top \right) W_{ij} + P_{ij} P_{ij}^\top \partial_{x_i}^\alpha W_{ij} \right], \quad (16)$$

$$\begin{aligned} \partial_{x_i}^{\alpha\beta} M_i = & \sum_j V_j \left[\left(\partial_{x_i}^{\alpha\beta} P_{ij} P_{ij}^\top + \partial_{x_i}^\alpha P_{ij} \partial_{x_i}^\beta P_{ij} + \partial_{x_i}^\beta P_{ij} \partial_{x_i}^\alpha P_{ij} + P_{ij} \partial_{x_i}^{\alpha\beta} P_{ij}^\top \right) W_{ij} + P_{ij} P_{ij}^\top \partial_{x_i}^{\alpha\beta} W_{ij} \right. \\ & \left. + \left(\partial_{x_i}^\alpha P_{ij} P_{ij}^\top + P_{ij} \partial_{x_i}^\alpha P_{ij} \right) \partial_{x_i}^\beta W_{ij} + \left(\partial_{x_i}^\beta P_{ij} P_{ij}^\top + P_{ij} \partial_{x_i}^\beta P_{ij} \right) \partial_{x_i}^\alpha W_{ij} \right], \end{aligned} \quad (17)$$

and $G = [1, 0, 0, \dots]^\top$. For more information on RK kernels, see Ref. [18]. The RK interpolant is defined as

$$f_{\text{RK}}(x) = \sum_j V_j f(x_j) U_j(x). \quad (18)$$

Letting \mathbb{P}_n be the space of polynomials with degree less than or equal to n , the RK kernels with correction order n exactly interpolate any function in \mathbb{P}_n ,

$$f_{\text{RK}}(x) = f(x), \quad f(x) \in \mathbb{P}_n.$$

The RK functions approximate delta functions ($U_j(x) \rightarrow \delta(x - x_j)$ as $H_j \rightarrow \infty$), so volume integrals of a smooth function and the kernel can be approximated as

$$\langle U_i, f \rangle = \int_V U_i f \approx f_i. \quad (19)$$

As only the values f_i are known (and not their derivatives), to calculate a derivative we first interpolate between the values using Eq. (18) and then take derivatives of the interpolant,

$$\langle U_i, \partial_x^\alpha f \rangle \approx \sum_j V_j f_j \langle U_i, \partial_x^\alpha U_j \rangle \approx \sum_j V_j f_j \partial_{x_i}^\alpha U_{ji}. \quad (20)$$

Second derivatives are performed similarly,

$$\langle U_i, \partial_x^{\alpha\beta} f \rangle \approx \sum_j V_j f_j \langle U_i, \partial_x^{\alpha\beta} U_j \rangle \approx \sum_j V_j f_j \partial_{x_i}^{\alpha\beta} U_{ji}. \quad (21)$$

For more complicated situations, as in Sec. 3.2, the the goal in deriving an RK derivative approximation is to isolate U_i so we can use Eq. (19) to evaluate the bilinear integral of U_i and whatever remains.

We need one more derivative to do SAAF transport (Sec. 3.1), which is the Hessian-like matrix $\partial^\alpha (g\partial^\beta f)$. To derive this approximation, we want to avoid derivatives multiplied by other derivatives, as then we would have to insert two interpolants for f and g , which would complicate the derivation and subsequent implementation considerably. The approximation starts by writing two different forms of the original derivative,

$$\partial^\alpha (g\partial^\beta f) = \partial^{\alpha\beta} (gf) - \partial^\beta g \partial^\alpha f - f \partial^{\alpha\beta} g, \quad (22)$$

$$\partial^\alpha (g\partial^\beta f) = g \partial^{\alpha\beta} f + \partial^\alpha g \partial^\beta f. \quad (23)$$

Averaging these two approximations, we get

$$\partial^\alpha (g\partial^\beta f) = \frac{1}{2} \left[\partial^{\alpha\beta} (gf) - f \partial^{\alpha\beta} g + g \partial^{\alpha\beta} f + \left(\partial^\alpha g \partial^\beta f - \partial^\beta g \partial^\alpha f \right) \right]. \quad (24)$$

If this identity is multiplied by the same vector twice, as it is for SAAF, then this term can be symmetrized without affecting its validity, since $k^\alpha k^\beta \partial^\alpha (g\partial^\beta f) = k^\alpha k^\beta \partial^\beta (g\partial^\alpha f)$. Under symmetrization, the term involving derivatives on both f and g in parenthesis disappears,

$$k^\alpha k^\beta \partial^\alpha (g\partial^\beta f) = \frac{1}{2} k^\alpha k^\beta \left[\partial^{\alpha\beta} (gf) - f \partial^{\alpha\beta} g + g \partial^{\alpha\beta} f \right]. \quad (25)$$

The RK approximation of this derivative is

$$\begin{aligned} k^\alpha k^\beta \langle U_i, \partial^\alpha (g\partial^\beta f) \rangle &= \frac{1}{2} k^\alpha k^\beta \left[\langle U_i, \partial^{\alpha\beta} (gf) \rangle - \langle U_i, f \partial^{\alpha\beta} g \rangle + \langle U_i, g \partial^{\alpha\beta} f \rangle \right] \\ &\approx \frac{1}{2} k^\alpha k^\beta \sum_j V_j (g_j f_j - g_j f_i + g_i f_j) \langle U_i, \partial^{\alpha\beta} U_j \rangle \\ &\approx \frac{1}{2} k^\alpha k^\beta \sum_j V_j (g_j f_j - g_j f_i + g_i f_j) \partial_{x_i}^{\alpha\beta} U_{ji} \end{aligned}$$

$$= \frac{1}{2} k^\alpha k^\beta \sum_j V_j (g_j + g_i) (f_j - f_i) \partial_{x_i}^{\alpha\beta} U_{ji}. \quad (26)$$

The extra $g_i f_i$ term that permits the factorization is equal to zero since $\sum_j V_j \partial_{x_i}^{\alpha\beta} U_{ji} = 0$. As far as we are aware, this form of the RK derivative is novel.

3. DISCRETIZATION OF THE TRANSPORT EQUATION

3.1. SAAF Transport

The SAAF transport equation is

$$- \Omega^\alpha \Omega^\beta \partial_x^\alpha \left(\frac{1}{\sigma_\tau} \partial_x^\beta \psi \right) + \sigma_\tau \psi = s - \Omega^\alpha \partial_x^\alpha \left(\frac{s}{\sigma_\tau} \right), \quad (27)$$

with the source

$$s = \tau \psi^n + \frac{1}{4\pi} \sigma_s \phi + q, \quad (28)$$

where Ω is the streaming direction, σ_s is the scattering cross section, σ_a is the absorption cross section, $\tau = 1/(c\Delta t)$, $d\sigma_\tau = \sigma_s + \sigma_a + \tau$, and q is the nonhomogeneous source. Equation 27 is multiplied by U_i and integrated,

$$\Omega^\alpha \Omega^\beta \left\langle U_i, \partial_x^\alpha \left(\frac{1}{\sigma_\tau} \partial_x^\beta \psi \right) \right\rangle + \langle U_i, \sigma_\tau \psi \rangle = \langle U_i, s \rangle - \Omega^\alpha \left\langle U_i, \partial_x^\alpha \left(\frac{s}{\sigma_\tau} \right) \right\rangle, \quad (29)$$

before the approximations in Eqs. (19), (20), and (26) are inserted,

$$- \Omega^\alpha \Omega^\beta \frac{1}{2} \sum_j V_j \left(\frac{1}{\sigma_{\tau,i}} + \frac{1}{\sigma_{\tau,j}} \right) (\psi_j - \psi_i) \partial^{\alpha\beta} U_{ji} + \sigma_{\tau,i} \psi_i = s_i - \Omega^\alpha \sum_j V_j \frac{s_j}{\sigma_{\tau,j}} \partial^\alpha U_{ji}. \quad (30)$$

3.2. SUPG Transport

The standard linear transport equation with backward Euler time differencing can be written as

$$\Omega^\alpha \partial_x^\alpha \psi_m + \sigma_\tau \psi = s, \quad (31)$$

where s is defined in Eq. (28). To discretize this equation with SUPG, Eq. (31) is multiplied by $U_i + \kappa_i \Omega^\alpha \partial_x^\alpha U_i$ and integrated,

$$\Omega^\alpha \langle U_i, \partial^\alpha \psi \rangle + \langle U_i, \sigma_\tau \psi \rangle + \kappa_i \Omega^\alpha \Omega^\beta \left\langle \partial^\beta U_i, \partial^\alpha \psi \right\rangle + \kappa_i \Omega^\alpha \langle \partial^\alpha U_i, \sigma_\tau \psi \rangle = \langle U_i, s \rangle + \kappa_i \Omega^\alpha \langle \partial^\alpha U_i, s \rangle. \quad (32)$$

The derivatives are moved away from the U_i terms through integration by parts and the surface integrals are discarded,

$$\Omega^\alpha \langle U_i, \partial^\alpha \psi \rangle + \langle U_i, \sigma_\tau \psi \rangle - \kappa_i \Omega^\alpha \Omega^\beta \left\langle U_i, \partial^{\alpha\beta} \psi \right\rangle - \kappa_i \Omega^\alpha \langle U_i, \partial^\alpha (\sigma_\tau \psi) \rangle = \langle U_i, s \rangle - \kappa_i \Omega^\alpha \langle U_i, \partial^\alpha s \rangle. \quad (33)$$

Finally, the integrals are performed as in Eqs. (19), (20), and (21) to get the discretized equation,

$$\sum_j V_j \left[(1 - \kappa_i \sigma_{\tau,j}) \Omega^\alpha \partial^\alpha U_{ji} - \kappa_i \Omega^\alpha \Omega^\beta \partial^{\alpha\beta} U_{ji} \right] \psi_j + \sigma_{\tau,i} \psi_i = s_i - \kappa_i \Omega^\alpha \sum_j V_j s_j \partial^\alpha U_{ji}. \quad (34)$$

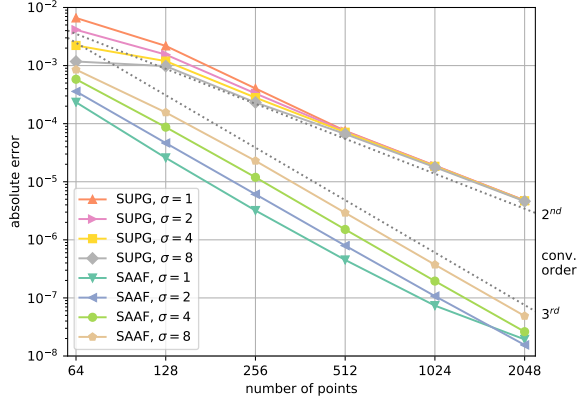


Figure 1: Absolute error for the purely absorbing problem for SAAF and SUPG for four values of the absorption cross section.

The stabilization coefficient κ is set to be the average distance between neighboring points, which for a function like the Gaussian means that the relative magnitudes of U_i and $\kappa_i \partial_x^\alpha U_i$ do not depend on the smoothing length H .

It is of note that for constant cross sections and $\kappa = 1/\sigma_\tau$ (where the effective mean free path is equal to the point spacing), the discretized SUPG and SAAF equations are exactly equal. If κ were taken to be spatially-dependent in the SUPG test function, the resulting equation is

$$\begin{aligned} \sum_j V_j \left[(1 - \kappa_j \sigma_{\tau,j}) \Omega^\alpha \partial^\alpha U_{ji} \psi_j - \frac{1}{2} \Omega^\alpha \Omega^\beta (\kappa_j + \kappa_i) (\psi_j - \psi_i) \partial^{\alpha\beta} U_{ji} \right] + \sigma_{\tau,i} \psi_i \\ = s_i - \Omega^\alpha \sum_j V_j \kappa_j s_j \partial^\alpha U_{ji}, \quad (35) \end{aligned}$$

which is exactly equal to the SAAF equation even with spatially-dependent cross sections if $\kappa = \sigma_\tau$. In practice, this equation does not perform as well as a constant κ_i . For a constant κ_i and a Gaussian-like kernel, the stabilization can be interpreted as upwinding the kernel. If κ is dependent on σ_τ or is spatially-dependent within a test function, then the shape of the test function will change based on the extent of other kernels or refinement in space or time.

4. RESULTS

We consider three test cases, a purely-absorbing slab in 1D with an analytic solution and steady-state and time-dependent manufactured solutions in 1D and 2D. Second-order RK corrections (e.g. in 2D a polynomial vector of $P^\top = [1, x, y, x^2, xy, y^2]$), a kernel support of six times the point spacing (see Ref. [20] for details), and Wendland 33 kernels [21] are used for all cases.

4.1. Purely Absorbing

The steady-state purely absorbing problem involves setting a boundary value for the angular flux, ψ_0 , incident on a purely-absorbing slab with an absorption cross section of σ_a . Given the distance from the

boundary x and the direction cosine $\mu = \Omega_x$, the analytic solution to this problem is

$$\psi = \psi_0 \exp\left(-\frac{\sigma_a x}{\mu}\right).$$

We consider each of SAAF and SUPG for four cross section values, $\sigma_a = 1, 2, 4, 8$, and calculate the absolute error of the numeric solution compared to the analytic,

$$\epsilon_{L_1} = \int_V |\psi_{\text{num}} - \psi_{\text{ana}}| \approx \sum_i V_i |\psi_{\text{num},i} - \psi_{\text{ana},i}|.$$

Figure 1 shows the error for all eight cases. As expected, the cases with higher cross sections have larger error as the density of points needed to resolve the steep solution is larger. The SUPG and SAAF results are consistent with second and third-order converge, respectively. In the next problem, the convergence orders swap, but it is unclear from the results that we have why that is. Possible reasons could be the difference in boundary and internal source treatments between SAAF and SUPG or a preference for SAAF toward problems with large gradients.

4.2. Steady-State Manufactured

This problem is a steady-state manufactured solution,

$$\psi_{\text{man}} = 1.2 + \prod_{\alpha=1}^{\text{dimension}} \cos(2\pi x^\alpha), \quad (36)$$

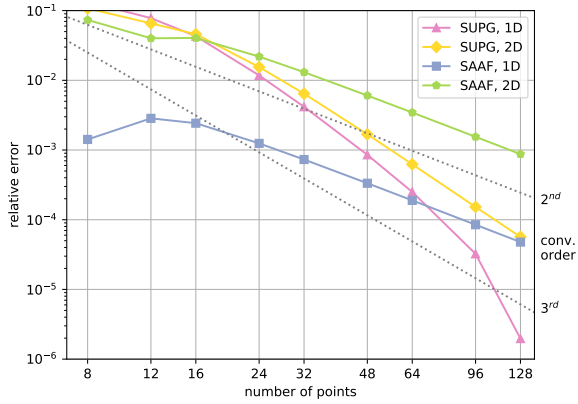
for each of SAAF and SUPG in 1D and 2D. This solution is inserted into the steady-state first-order transport equation [Eq. (31) with $\tau \rightarrow 0$] and solved for q , after which this q is used in a transport calculation to calculate a numeric flux, ψ_{numeric} . We then calculate the volume-integrated relative L_2 error between the manufactured and numeric solutions,

$$\epsilon_{L_2, \text{rel}} = \frac{\int_V |\psi_{\text{num}} - \psi_{\text{man}}|}{\int_V \psi_{\text{man}}} \approx \frac{\sum_i V_i |\psi_{\text{num},i} - \psi_{\text{man},i}|}{\sum_i V_i \psi_{\text{man},i}}.$$

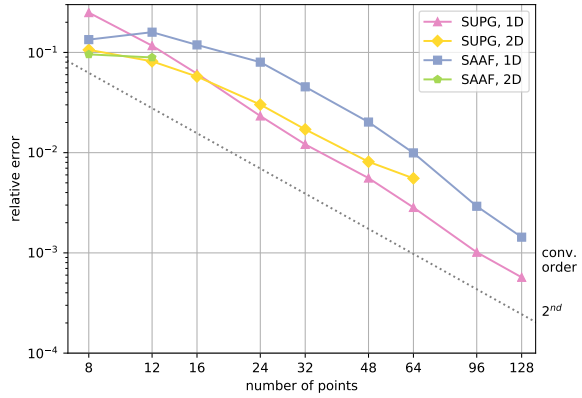
The points are placed uniformly in one case and are randomly perturbed by up to 0.2 times the point spacing in the other.

Figure 2 shows the error for the uniform and non-uniform cases. For uniform points, the SAAF transport converges with second-order accuracy. The SUPG transport convergence with third-order accuracy in 2D and spectral accuracy in 1D. For non-uniform points, the GMRES transport solver with ILUT preconditioning in the more refined SUPG cases and most of the SAAF cases did not converge to the specified tolerance of 10^{-14} within 1,000 iterations, so these points are not included on the plot. The SUPG results in 1D and 2D as well as the SAAF results in 1D imply second-order convergence.

The SAAF results in 2D are particularly sensitive to random perturbations in point locations and do not converge for a majority of the cases with randomized point locations. The SUPG results in 2D perform better but still struggle to converge using Trilinos GMRES solver with ILUT preconditioning [22]. For problems in which the point locations are not chosen (e.g. in a simulation coupled with hydrodynamics), this could present issues. When using a direct solver, the results continue to converge, but this is impractical to do for realistic problems. General-purpose AMG preconditioners, such as BoomerAMG in Hypr [23], fare worse than the ILUT preconditioners. Because of this, additional work needs to be done on selecting proper solvers for the equations; special-purpose preconditioners such as the transport solver pAIR described in Ref. [24] may help.

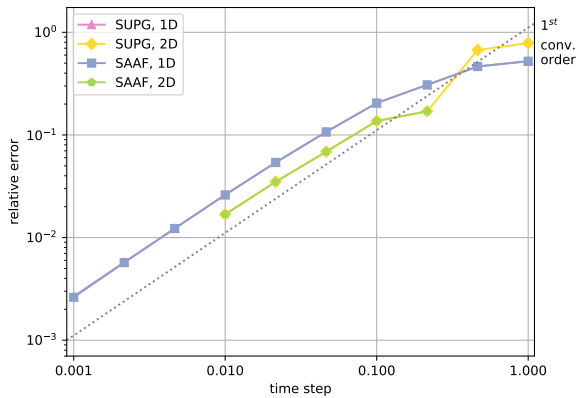


(a) Uniform point distribution.

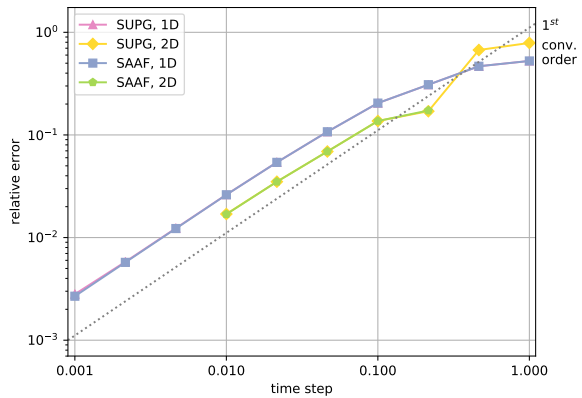


(b) Non-uniform point distribution.

Figure 2: Relative error for the steady-state sinusoidal manufactured solution for SAAF and SUPG in 1D and 2D. The points that are missing in the non-uniform case represent simulations that did not converge.



(a) Uniform point distribution.



(b) Non-uniform point distribution.

Figure 3: Relative error for the time-dependent sinusoidal manufactured solution for SAAF and SUPG in 1D and 2D. The SAAF results for the two largest time steps in 2D did not converge and are excluded.

4.3. Time-Dependent Manufactured

This problem is similar to the steady-state version except with a time-dependent term added into the manufactured solution,

$$\psi_{\text{man}} = 1.2 + \prod_{\alpha=1}^{\text{dimension}} \cos(2\pi(x^\alpha + t)),$$

that also results in a time-dependent source. The number of points is held constant at 64 along each dimension. The time step is chosen and held constant throughout the simulation. As before, the points are held constant for one set of tests and randomly perturbed by up to 0.2 times the point spacing in the other set. The error is calculated as in the previous test.

Figure 3 shows the convergence results. There is less than one percent difference between the solutions with randomized and non-randomized points, which indicates that the error in the time-dependent case is dominated by the time step. Both the uniform and randomized sets of tests are consistent with first-order convergence in time, as expected with our fully-implicit time discretization. The solver struggles to converge for SAAF when the time step is large. See the steady-state section for a discussion on preconditioners and convergence.

5. CONCLUSIONS

The SAAF and SUPG transport equations are discretized using RK with a combination of familiar derivatives and a novel second derivative. The resulting equations involve only evaluations of kernels and physical data at the nodal centers. With second-order RK kernels, the uniform and non-uniform results are consistent with at least second-order convergence. The SAAF results for non-uniform points struggle to converge in 2D. While some of these problems are allayed by the effective absorption in the time-dependent problem, the SAAF and SUPG solvers may benefit from specialized preconditioners. In order to extend the results to higher order, a larger kernel support would be needed that would exacerbate these issues. Once the solvers are appropriately preconditioned, this method would be attractive for coupling to an SPH or CRKSPH simulation. The discretization is similar and the evaluations require no more data than the original SPH calculation except the cross sections at the evaluation nodes.

ACKNOWLEDGEMENTS

This work was performed under the auspices of the U.S. Department of Energy by Lawrence Livermore National Laboratory under Contract DE-AC52-07NA27344. LLNL-CONF-819823.

References

- [1] J. J. Monaghan. “Smoothed particle hydrodynamics.” *Reports on progress in physics*, **volume 68**(8), p. 1703 (2005).
- [2] S. C. Whitehouse and M. R. Bate. “Smoothed particle hydrodynamics with radiative transfer in the flux-limited diffusion approximation.” *Monthly Notices of the Royal Astronomical Society*, **volume 353**(4), pp. 1078–1094 (2004).
- [3] S. C. Whitehouse, M. R. Bate, and J. J. Monaghan. “A faster algorithm for smoothed particle hydrodynamics with radiative transfer in the flux-limited diffusion approximation.” *Monthly Notices of the Royal Astronomical Society*, **volume 364**(4), pp. 1367–1377 (2005).

- [4] S. Viau, P. Bastien, and S.-H. Cha. “An implicit method for radiative transfer with the diffusion approximation in smooth particle hydrodynamics.” *The Astrophysical Journal*, **volume 639**(1), p. 559 (2006).
- [5] L. Mayer, G. Lufkin, T. Quinn, and J. Wadsley. “Fragmentation of gravitationally unstable gaseous protoplanetary disks with radiative transfer.” *The Astrophysical Journal Letters*, **volume 661**(1), p. L77 (2007).
- [6] M. Petkova and V. Springel. “An implementation of radiative transfer in the cosmological simulation code GADGET.” *Monthly Notices of the Royal Astronomical Society*, **volume 396**(3), pp. 1383–1403 (2009).
- [7] B. R. Bassett, J. M. Owen, and T. A. Brunner. “Efficient smoothed particle radiation hydrodynamics I: Thermal radiative transfer.” *arXiv preprint arXiv:200111606* (2020).
- [8] H. Sadat. “On the use of a meshless method for solving radiative transfer with the discrete ordinates formulations.” *Journal of Quantitative Spectroscopy and Radiative Transfer*, **volume 101**(2), pp. 263–268 (2006).
- [9] H. Sadat, C.-A. Wang, and V. Le Dez. “Meshless method for solving coupled radiative and conductive heat transfer in complex multi-dimensional geometries.” *Applied Mathematics and Computation*, **volume 218**(20), pp. 10211–10225 (2012).
- [10] M. Kindelan, F. Bernal, P. González-Rodríguez, and M. Moscoso. “Application of the RBF meshless method to the solution of the radiative transport equation.” *Journal of Computational Physics*, **volume 229**(5), pp. 1897–1908 (2010).
- [11] L. Liu and J. Tan. “Least-squares collocation meshless approach for radiative heat transfer in absorbing and scattering media.” *Journal of Quantitative Spectroscopy and Radiative Transfer*, **volume 103**(3), pp. 545–557 (2007).
- [12] J. Zhao, J. Tan, and L. Liu. “A second order radiative transfer equation and its solution by meshless method with application to strongly inhomogeneous media.” *Journal of Computational Physics*, **volume 232**(1), pp. 431–455 (2013).
- [13] S. Kashi, A. Minuchehr, A. Zolfaghari, and B. Rokrok. “Mesh-free method for numerical solution of the multi-group discrete ordinate neutron transport equation.” *Annals of Nuclear Energy*, **volume 106**, pp. 51–63 (2017).
- [14] L. Liu and J. Tan. “Meshless local Petrov-Galerkin approach for coupled radiative and conductive heat transfer.” *International journal of thermal sciences*, **volume 46**(7), pp. 672–681 (2007).
- [15] B. Bassett and B. Kiedrowski. “Meshless local Petrov-Galerkin solution of the neutron transport equation with streamline-upwind Petrov-Galerkin stabilization.” *Journal of Computational Physics*, **volume 377**, pp. 1–59 (2019).
- [16] J. Morel and J. McGhee. “A self-adjoint angular flux equation.” *Nuclear Science and Engineering*, **volume 132**(3), pp. 312–325 (1999).
- [17] C. Pain, M. Eaton, R. Smedley-Stevenson, A. Goddard, M. Piggott, and C. De Oliveira. “Streamline upwind Petrov-Galerkin methods for the steady-state Boltzmann transport equation.” *Computer methods in applied mechanics and engineering*, **volume 195**(33-36), pp. 4448–4472 (2006).
- [18] W. K. Liu, S. Jun, and Y. F. Zhang. “Reproducing kernel particle methods.” *International journal for numerical methods in fluids*, **volume 20**(8-9), pp. 1081–1106 (1995).
- [19] N. Frontiere, C. D. Raskin, and J. M. Owen. “CRKSPH—A Conservative Reproducing Kernel Smoothed Particle Hydrodynamics Scheme.” *Journal of Computational Physics*, **volume 332**, pp. 160–209 (2017).

- [20] J. M. Owen. “ASPH modeling of material damage and failure.” Technical report, Lawrence Livermore National Laboratory (2010).
- [21] H. Wendland. “Piecewise polynomial, positive definite and compactly supported radial functions of minimal degree.” *Advances in computational Mathematics*, **volume 4**(1), pp. 389–396 (1995).
- [22] M. A. Heroux, R. A. Bartlett, V. E. Howle, R. J. Hoekstra, J. J. Hu, T. G. Kolda, R. B. Lehoucq, K. R. Long, R. P. Pawlowski, E. T. Phipps, et al. “An overview of the Trilinos project.” *ACM Transactions on Mathematical Software (TOMS)*, **volume 31**(3), pp. 397–423 (2005).
- [23] R. D. Falgout and U. M. Yang. “hypre: A library of high performance preconditioners.” In *International Conference on Computational Science*, pp. 632–641. Springer (2002).
- [24] J. Hanophy, B. S. Southworth, R. Li, T. Manteuffel, and J. Morel. “Parallel Approximate Ideal Restriction Multigrid for Solving the SN Transport Equations.” *Nuclear Science and Engineering*, **volume 194**(11), pp. 989–1008 (2020).